WARSAW UNIVERSITY OF TECHNOLOGY Index 351733
FACULTY OF CIVIL ENGINEERING
COMMITTEE FOR CIVIL AND WATER ENGINEERING
POLISH ACADEMY OF SCIENCES ISSN 1230-2945

DOI: 10.24425/ace.2025.154128
ARCHIVES OF CIVIL ENGINEERING
Vol. LXXI ISSUE 2 2025
pp. 393–412

Research paper

Research on static load test of segmental-assembled steel temporary beam buttress of railway line

Wenlong Ma[1], Yucai Ning[2], Ronghua Ge[3], Bo Shen[4], Yan Wang[5], Hanqing Zhuge[6]

Abstract: In order to reduce the self weight of railway line temporary beam buttresses and improve their construction convenience and reusability, this paper proposes the segmental-assembled steel temporary beam buttress. This kind of supporting pier is composed of three steel box segments, which are assembled through connecting plates and bolts. This article processed and produced a 1:4 scaled test specimen of this new-type buttress. The mechanical behavior and failure mode of the specimen was studied by applying a vertical static load equivalent to that transmitted by the temporary beam. According to the vertical load-displacement curve of the test, it can be seen that the specimen did not experience local buckling or overall instability during the loading process, and the overall structural performance is strong. The ultimate bearing capacity of the test component is 388 kN. The assemble joints between adjacent steel box segments are the weak region of the structure. The construction difficulty for the 1/4 scale test specimen may lead to the asymmetric deflection. The main failure modes are the punching failure of the steel plate near the bolt hole and shearing failure of bolts caused by the continuous increase of the joint gap width. It is indicated that the bending resistance of the joint is relatively low and needs to be properly strengthened during the design process. This study provides important support for the design and application of new-type segmental-assembled temporary beam buttress.

Keywords: bridge engineering, segmental-assembled, static load test, steel structure, temporary beam buttress

[1]MSc., Eng., Senior Engineer, Hangzhou Railway Design Institute Co.,Ltd., e-mail: mawl@hztlsjy.com, ORCID: 0009-0005-8653-746X
[2]MSc., Eng., Hangzhou Railway Design Institute Co., LTD, e-mail: ningyc@hztlsjy.com, ORCID: 0009-0009-3469-7540
[3]MSc., Eng., Hangzhou Railway Design Institute Co., LTD, e-mail: gerh@hztlsjy.com, ORCID: 0009-0009-2725-3511
[4]MSc., Eng., Zhejiang Railway Investment Construction Engineering Co., LTD, e-mail: 249831528@qq.com, ORCID: 0009-0005-6734-913X
[5]PhD., Eng. Associate Professor, Zhejiang Sci-Tech University, e-mail: an_wangyan@zstu.edu.cn, ORCID: 0000-0001-5664-3994
[6]PhD., Eng., Zhejiang University of Science and Technology, e-mail: 120043@zust.edu.cn, ORCID: 0000-0002-1856-7115

1. Introduction

In the railway engineering, interchange project between urban road and existing railway are numerous and critical [1,2]. The design scheme of underpass culvert is preferred [3]. When the road adopts the scheme of underpass culvert under the existing railway, the large-span jacking frame bridge is mostly used [4]. In the construction process of jacking method, it is necessary to set up temporary beams on the existing railway, and before setting up the temporary beams, it is necessary to pour reinforced concrete temporary beam buttresses. The existing reinforced concrete temporary beam buttresses have defects such as heavy load, slow construction period, inconvenient demolition, and difficulty to reuse [5]. At the same time, the construction process has a great impact on the existing railway [5], which is not in line with China's green and double-carbon development concept. Some scholars have proposed optimization measures for the design methods and construction techniques of temporary beam buttresses [6], but there is still a lack of research on the improvement of the material types and structural forms of temporary beam buttresses themselves. At present, utilizing the lightweight, high-strength, and green characteristics of steel structures, steel-box type portal piers have been used in multiple cross line bridges. The kind of piers has characteristics such as easy construction, clear stress, and good structural universality. Relevant research is also relatively mature. For example, Sun et al. [7] conducted the performance research on key components of large-span steel box gantry pier structures. Tao et al. [8] explores and analyzes the structural form and design keys of portal piers with steel cap beams based on multiple design examples of long railway trunk lines.

In order to reduce the self weight of the temporary beam buttresses to a greater extent, shorten the construction period, and improve their reusability, this article attempts to use thin-walled box shaped steel structures as the basic structural form of the temporary beam buttresses for the railway line. The mechanical characteristics of the steel-structure temporary beam buttress and the steel cap beam of portal piers are similar. However, to be reusable, the temporary beam buttress must be easy to transport, install, and disassemble on site. Thus, the overall steel structure form is difficult to be used. The steel-structure temporary beam buttresses can only be assembled in multiple segments. At present, many studies have been conducted on the mechanical behavior and seismic performance of precast concrete and precast steel-tube concrete segmental assembled bridge piers. For example, Chou at al. [9] studied the hysteretic properties of post-tensioned precast concrete-filled tube segmental bridge columns with unbonded strands through quasi-static tests. Zhang et al. [10] studied the seismic performance of the damaged precast segmental bridge columns, which were reinforced with the UHPC jacket, under combined cyclic loading and constant axial loading. A novel precast segmental bridge column was proposed in literature [11] to achieve a better durability performance in the aggressive coastal environment. As for steel structures, Fan et al. [12] studied the axial loading behavior of deconstructable bolt spliced square steel tubular columns. However, there have been no relevant reports on the bending mechanical behavior of segmental assembled steel structures.

This article proposes a new type of temporary beam buttress for railway, which is steel structural and segmental-assembled. In this structure, the entire temporary beam buttress is divided into three steel box components, which are assembled through connecting plates and

bolts. By applying a vertical static load to the scaled test specimen, which is equivalent to that transmitted from the temporary beam, the overall mechanical state of the test specimen is thoroughly studied. By measuring the strain at key positions and joint gap width changes during the loading process, the failure mode and weak parts of the steel structure beam buttress component are clarified. This research provides important support for the design and application of the new segmental-assembled steel temporary beam buttresses.

2. Experimental loading

2.1. Segmental-assembled steel buttress specimen and testing device

Based on the testing ability, the segmental-assembled steel buttress specimen is determined to be processed in the 1:4 reduced scale. The total length of the buttress specimen is 2.62 m, using 50 cm (width) × 37.5 cm (height) rectangular cross section. The designed geometric size of the simple supported beam with the box section can ensure the bending-torsional overall stability [13]. The components are assembled in three sections, with two end sections and one middle section, which are all 87.5 cm long. The connecting steel plates are installed inside and outside the mother plate. All the steel plates are made of Q345qC steel, which is commonly used in Chinese bridge engineering. The mechanical properties of Q345qC steel have been calibrated by the authors' research group [14, 15]. The elastic modulus is 204 500 MPa and the yield strength is 391.2 MPa. The mother plates, the inside and outside connecting plates are connected together by Chinese M8 high-strength bolts. The typical cross-sectional diagram and schematic diagram of the joint part are shown in Figure 1, and the longitudinal diagram is shown in Figure 2.

The box-section segments contain longitudinal stiffeners and transverse diaphragms. Four longitudinal stiffeners are set on the top and bottom plates, with a spacing of 10cm. Two longitudinal stiffeners are set on the web plates, with a spacing of 12.5 cm and a width of 50 cm. The spacing between transverse diaphragms is 20–22.5 cm. The size of local transverse

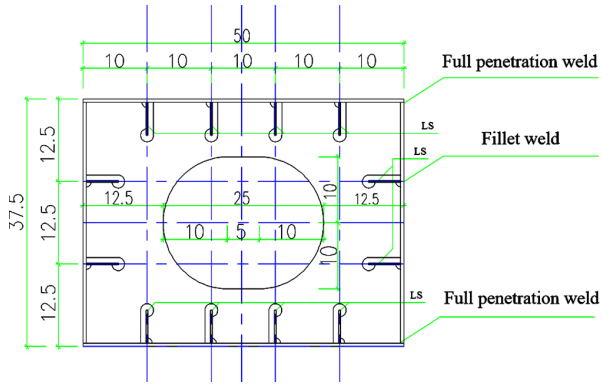

(a) Facade diagram

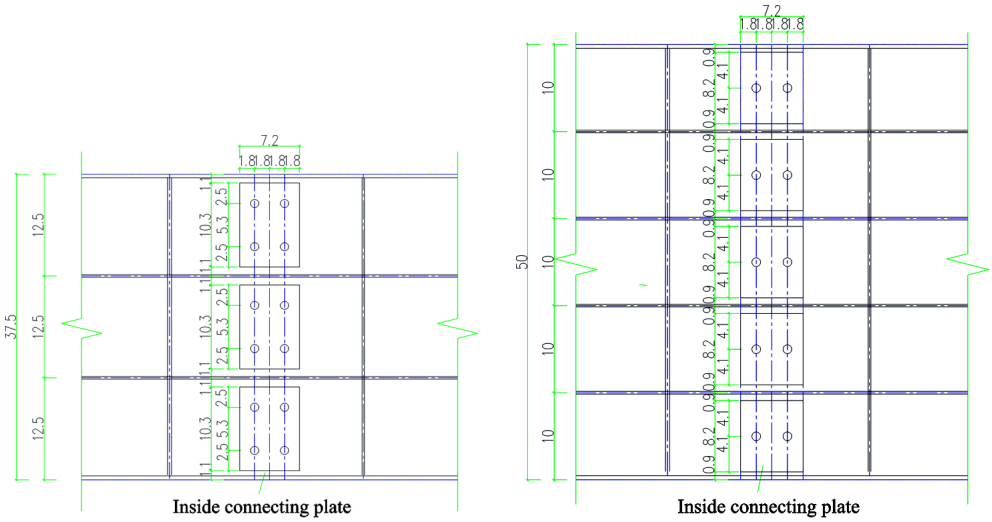

(b) Joint elevation diagram (c) Joint plane diagram

Fig. 1. Typical cross-sectional diagram and schematic diagram of the joint (unit: cm)

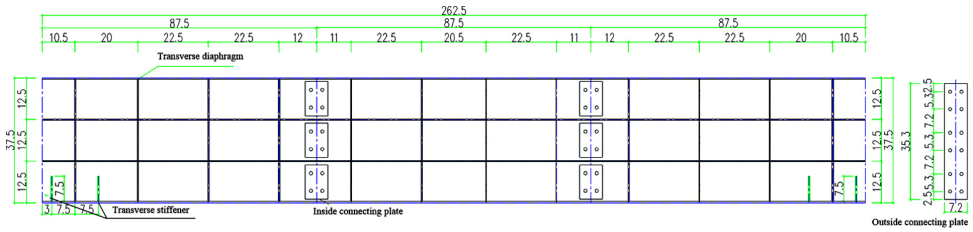

(a) Facade diagram

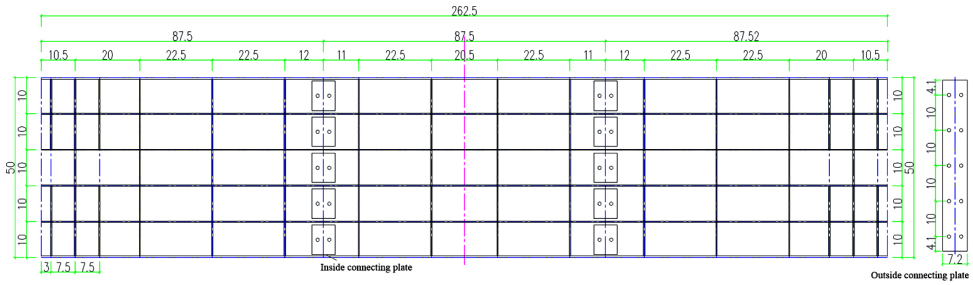

(b) Plane diagram

Fig. 2. Longitudinal diagram of buttress specimen (unit: cm)

stiffeners at the support is 7.5 × 19.35 cm. The thickness of local transverse stiffeners at the support is 6 mm. The thickness of the box plates is 5 mm, and the thickness of the connecting plates is also 5 mm. The thickness of the transverse diaphragms at the connection between the

support and the specimen and the connection between the temporary beam and the specimen is 5 mm, while the thicknesses of the other longitudinal stiffeners and transverse diaphragms are 3 mm. The longitudinal stiffeners and transverse diaphragms of the segmental-assembled steel buttress can ensure the local stability of the webs and the compression flanges [13].

In order to analyze the mechanical characteristics and deformation law of the new-type buttress, the experiment adopts the four-point-bending loading mode. This loading form can reproduce the actual force and deformation of the buttress under the vertical load transmitted by the actual temporary beam, which is conducive to observing and analyzing the strain, deformation, and joint gap development of the buttress at each stage of loading. The schematic diagram of the specimen loading is shown in Figure 3. The experiment was conducted at the experimental center of the College of Civil and Architectural Engineering, Zhejiang University of Science and Technology. The photos of the experimental site are shown in Figure 4.

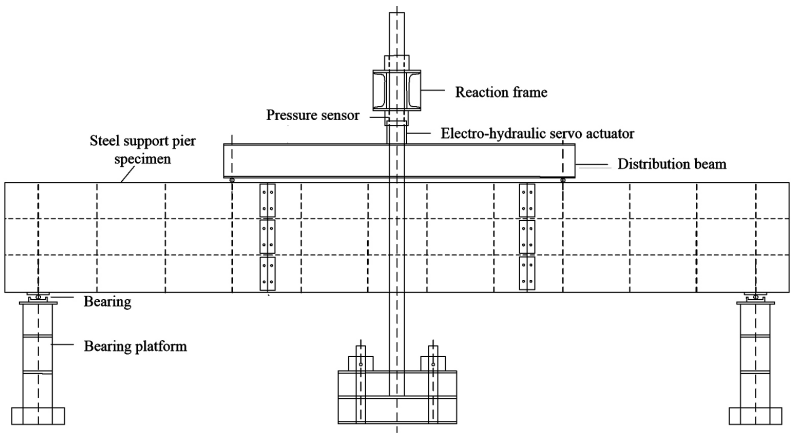

(a) Facade diagram

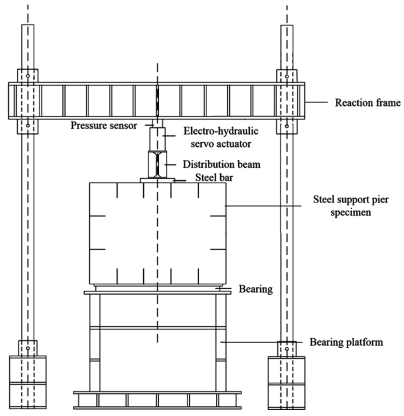

(b) Elevation diagram

Fig. 3. Schematic diagram of test loading

(a) Placement and positioning

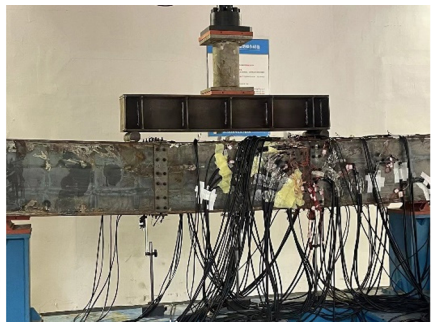

(b) Ready to load

Fig. 4. Photos of the test site; (a) Placement and positioning (b) Ready to load

This experiment uses an electro-hydraulic servo actuator and a loading reaction frame to implement loading. The maximum load which can provided is 500 kN. The electro-hydraulic servo actuator is calibrated in advance through a force sensor and can automatically collect vertical loads at a frequency of 0.5 Hz. In addition, the equipment for collecting experimental data includes 120 Ohm welding free steel bar strain gauges with the measuring range from –20000 με to 20000 με and static strain data acquisition box.

2.2. Loading program

In this experiment, load control loading was used first. When the specimen is unable to hold the imposed load, the loading method was changed to displacement control loading. When the load of the specimen drops to about 80% of the maximum load or the specimen is not suitable for further loading, the loading is stopped and the test is finished. During the experiment, preloading is carried out first to eliminate partial gaps in bolt holes and other positions. The maximum load applied during preloading is 55 kN. During formal loading, a graded loading mechanism is adopted, with each level of load increment set at 10 kN. After each level of load is loaded and the deformation stabilizes, the vertical displacements and joint opening data are recorded.

2.3. Monitoring point arrangement

During the experiment, to measure the deflection of the beam, dialgages were installed at the 1/4 span, mid span and 3/4 span positions, and a vernier caliper was used to measure the gap width of the joint. To measure the stress distribution, strain gauges and strain rosette gauges are arranged at key points of the component, including the critical sections of the mother plates, longitudinal stiffeners, and transverse diaphragms, as well as the positions of the mother plates and the connecting plates near the bolt holes. The specific arrangement positions of strain gauges near the bolt positions of each steel plate are shown in the following Figure 5.

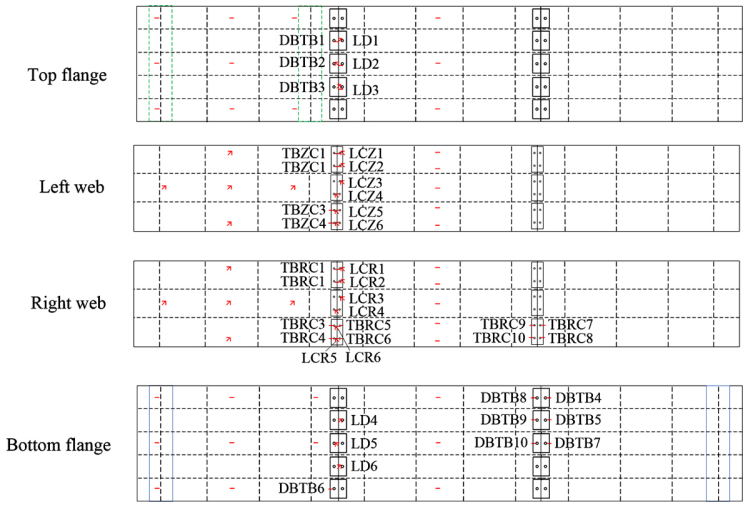

(a) Layout of strain gauges for key sections of mother plates

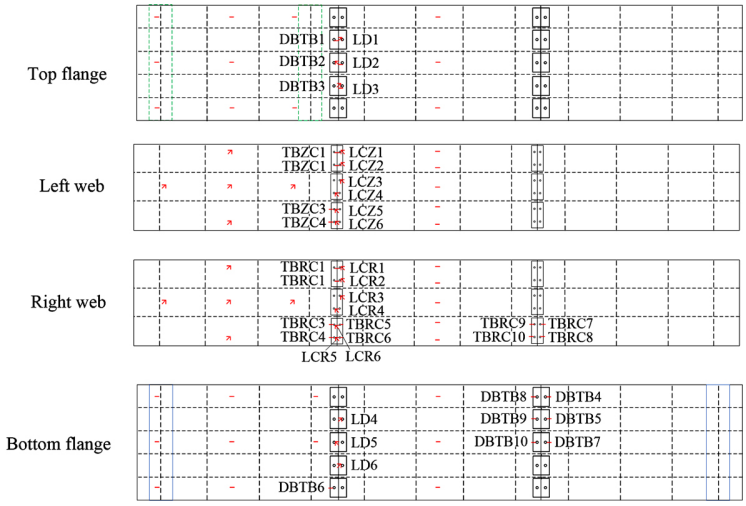

(b) Layout of strain gauges and strain rosette gauges near bolt holes for mother plates and connecting plates

Fig. 5. Schematic diagram of strain gauge and strain rosette gauge arrangement; (a) Layout of strain gauges for key sections of mother plates, longitudinal stiffeners, and transverse diaphragms; (b) Layout of strain gauges and strain rosette gauges near bolt holes for mother plates and connecting plates (Annotation: D – top flange; d – bottom flange; CZ – left web; CR – right web; H – transverse diaphragm; J – longitudinal stiffener; LD(1~3) – top flange near bolts; LD(4~6) – bottom flange near bolts; DBTB(1~3) – top connecting plate; DBTB(4~10) – bottom connecting plate; LCZ – left web near bolts; TBZC – left connecting plate; LCR – right web near bolts; TBRC – right connecting plate)

3. Experimental results and analysis

3.1. Load displacement curve results and experimental phenomena

The load-displacement curve is an important basis for measuring the vertical bearing capacity and stiffness of a structure. The vertical load-displacement curve of the steel-structure temporary beam buttress is shown in Figure 6(a). The results showed that a complete load-displacement curve of the scaled test specimens of the steel-structure temporary beam buttress was obtained in this experiment, and the vertical ultimate bearing capacity of is 388 kN.

At the beginning of the loading stage, the specimen maintained a high stiffness, but the stiffness significantly decreased when the load reached around 60 kN. This is because the test components were assembled by three independent steel box components through bolts and the maximum preload is 55 kN. The first batch of bolt hole gaps were already tightened during

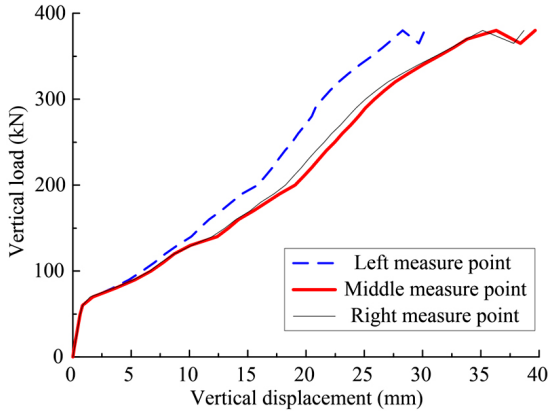

(a) The vertical load-displacement curve of the specimen

(b) The final failure mode of the specimen

Fig. 6. The vertical load-displacement curve and the final failure mode of the specimen

preloading. When the load is larger than 60 kN, other bolt holes were further tightened, so the vertical displacement includes the displacement caused by the loosening of the bolt holes. When the load reaches around 200 kN, the stiffness begins to increase, indicating that all bolt holes have been tightened and the specimen has entered the overall load-bearing working state. After the load reaches around 200 kN, the stiffness began to decrease again, which is due to the gradual plastic deformation of the mother plate near the bolt holes, and the plastic deformation area continued to increase. When the load increased to 380 kN, accompanied by a sound, a bolt at the bottom plate was cut and collapsed, and the bearing capacity quickly decreased to around 360 kN and stabilized.

On the premise of ensuring safety, the load continued until 388 kN, and multiple noises occurred continuously. It was observed that the bottom flanges and webs near multiple bolt holes of were severely sheared and damaged. At the same time, multiple bolts were sheared and collapsed, causing a sharp decrease in the bearing capacity of the specimen and the loading was terminated. The final failure mode of the specimen is shown in Figure 6(b). It can be seen from the figure that the specimen did not experience local buckling or overall instability during the loading process.

3.2. Vertical load-strain curve results

This section draws load-strain history curve based on the measuring results of all strain gauges under each level of loading. The specific strain situation is as follows.

The strain at the top flanges and bottom flanges is relatively small, and almost all of the results are compressive. Due to not reaching the yield strain, the strain at the top flanges increases linearly with the increase of load. At the same time, the strain of the mid span sections (D7, D8, D9) is significantly larger, because the mid span section is in the pure bending section with the maximum bending moment. The strain of each section increases with the increase of the distance to the support, which is consistent with the distribution of bending moment. The strain at the bottom flanges is similar to that at the top flanges, and it is relatively small, with almost all showing tensile strain. Due to not reaching the yield strain, the strain at the bottom flanges increases linearly with the increase of load. At the same time, the strain of the mid span section (d7, d8, d9) is significantly larger, because the mid span section is in the pure bending section, with the maximum bending moment, and the strain is relatively larger compared to other sections.

Five strain rosette gauges, namely CZ1–CZ5, were pasted on the left web at the section near the support. The strain at each measuring point is relatively small and the trend of change is similar. The longitudinal strain, vertical strain, 45°strain, and shear strain at each measuring point have not reached the yield strain, so they basically increase linearly with the increase of load. The shear strain of each strain flower is greater than the longitudinal strain, indicating that the web plate mainly bears shear action. The shear strain of CZ2–CZ4 is similar, indicating that the shear stress is uniformly distributed along the height direction of the section. The shear

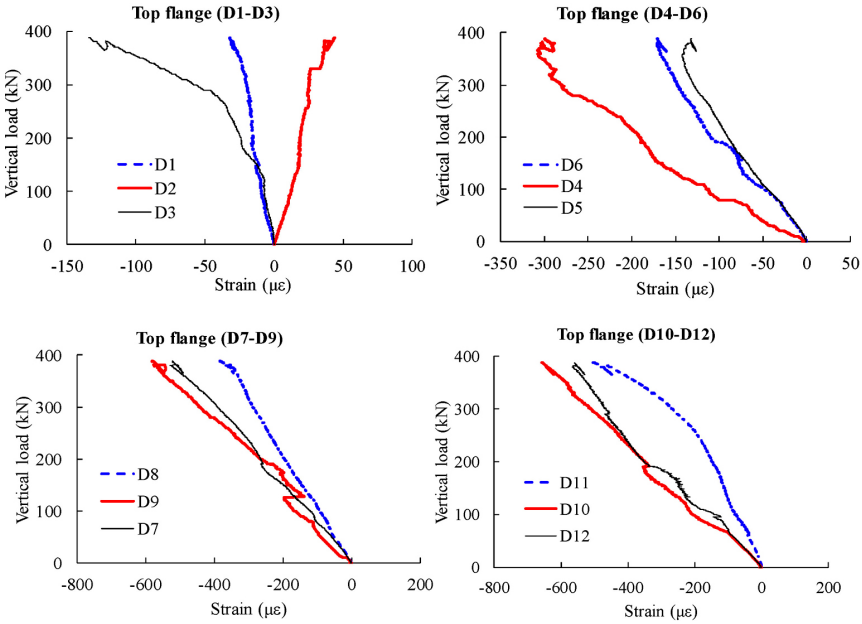

Fig. 7. Vertical load-strain curve at the top flanges

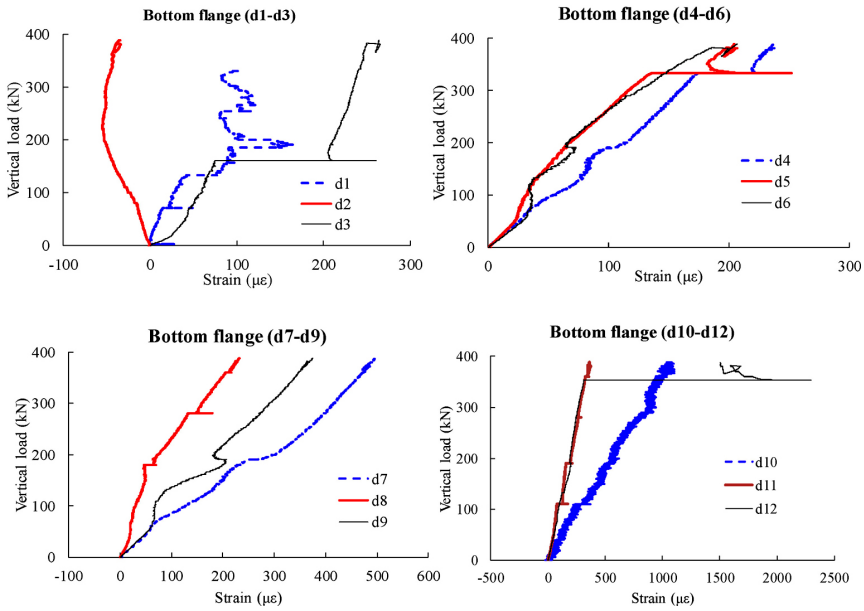

Fig. 8. Vertical load-strain curve at the bottom flanges

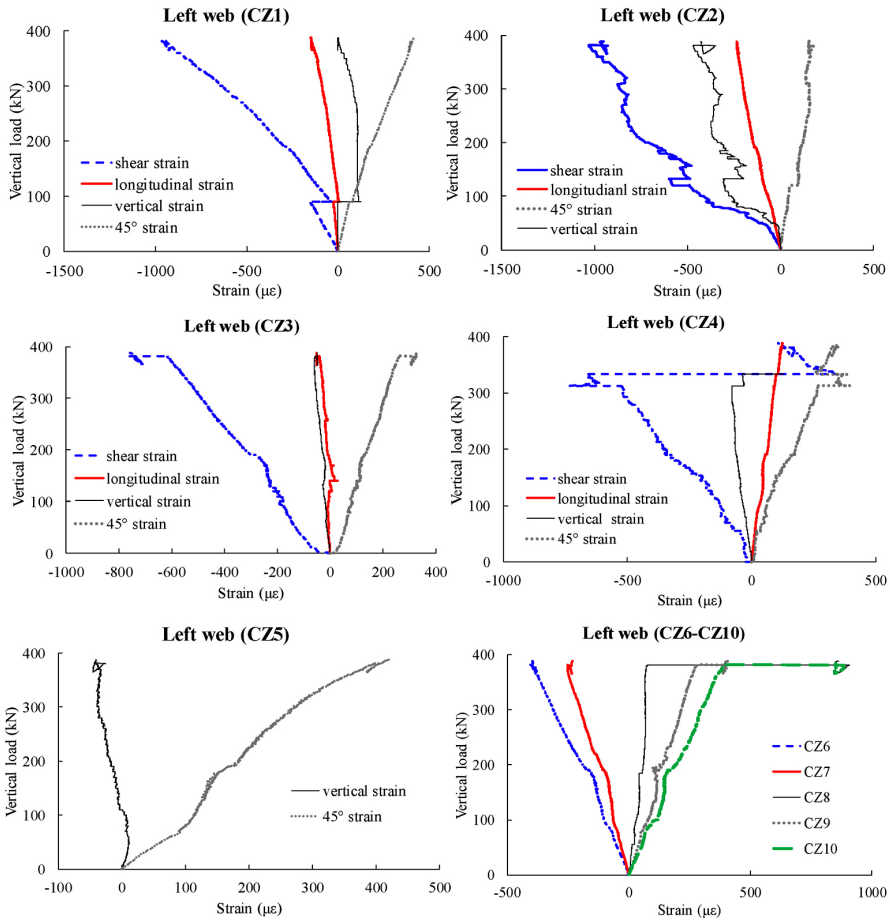

Fig. 9. Load-strain results of the left web (Annotation: longitudinal strain gage of CZ5 is open circuit)

strains of CZ1 and CZ3 are similar, because the shear forces of each section on the outer side of the pure bending section are equal.

Five strain gauges were pasted along the height of the cross-section at the mid-span position of the middle section on the left web, with CZ6–CZ10 from top to bottom. Each strain gauge has not reached the yield strain, so it basically increases linearly with the increase of load. Among them, CZ6 and CZ7 are compressive strains, CZ9 and CZ10 are tensile strains, and CZ8 strain is very small, so the neutral axis is basically located at the height of the section center.

As given in Figure 10, the strain distribution and variation patterns at various locations on the right webs are very similar with the those on the left webs, and will not be repeated here. This further confirms that the loading process in this experiment is symmetrical along the transverse direction, and there will be no out of plane deformation. The stress is also uniformly distributed along the transverse direction.

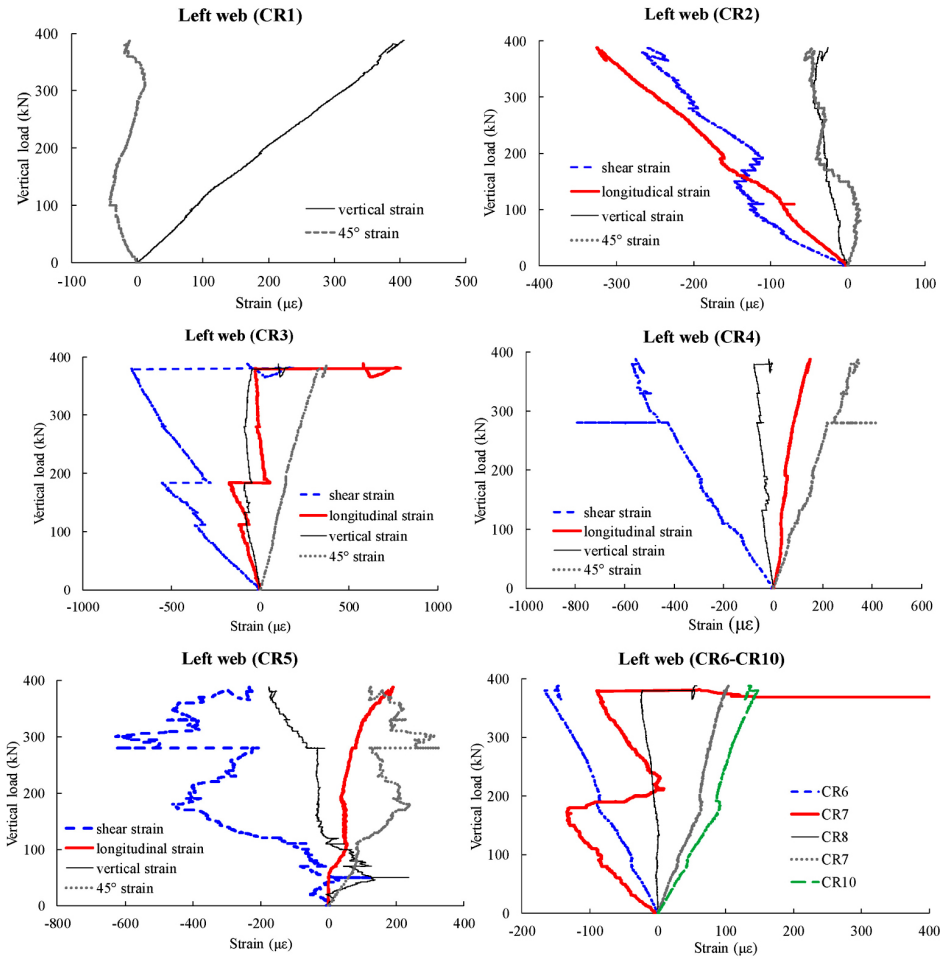

Fig. 10. Load-strain results of the right web (Annotation: longitudinal strain gage of CR1 is open circuit)

Three strain rosette gauges are arranged on the transverse diaphragms of the edge segment, in the sections near the support and near the joint, respectively. As shown in the Figure 11, the strain at the point H1 reaches about 2000 με when the load reaches about 340 kN. Afterwards, the slope of load-strain curve significantly decreases, indicating that the steel enters the plastic stage where significant plastic deformation will occur. The remaining measuring points are basically within the elastic range, and the strain increases linearly with the load. Since H1–H2 and H6–H7 are located near longitudinal stiffeners, the local stress state is significantly constrained by the stiffeners, and the stress states are different, and may even reach a plastic state (H1). The H5 and H10 measuring points are both located near the manhole and are less constrained, so the stress states of the two measuring points are very similar. Strain rosette gauges were arranged on the two longitudinal stiffeners at the edge segment, in the section

near the support and the joint surface. As shown in the Figure 12, the strain on the longitudinal stiffeners has not reached the yield strain, and the strain increases linearly with the load, indicating that all measuring points on the longitudinal stiffeners are within the elastic range. Meanwhile, the stress states of each measuring point are also relatively close.

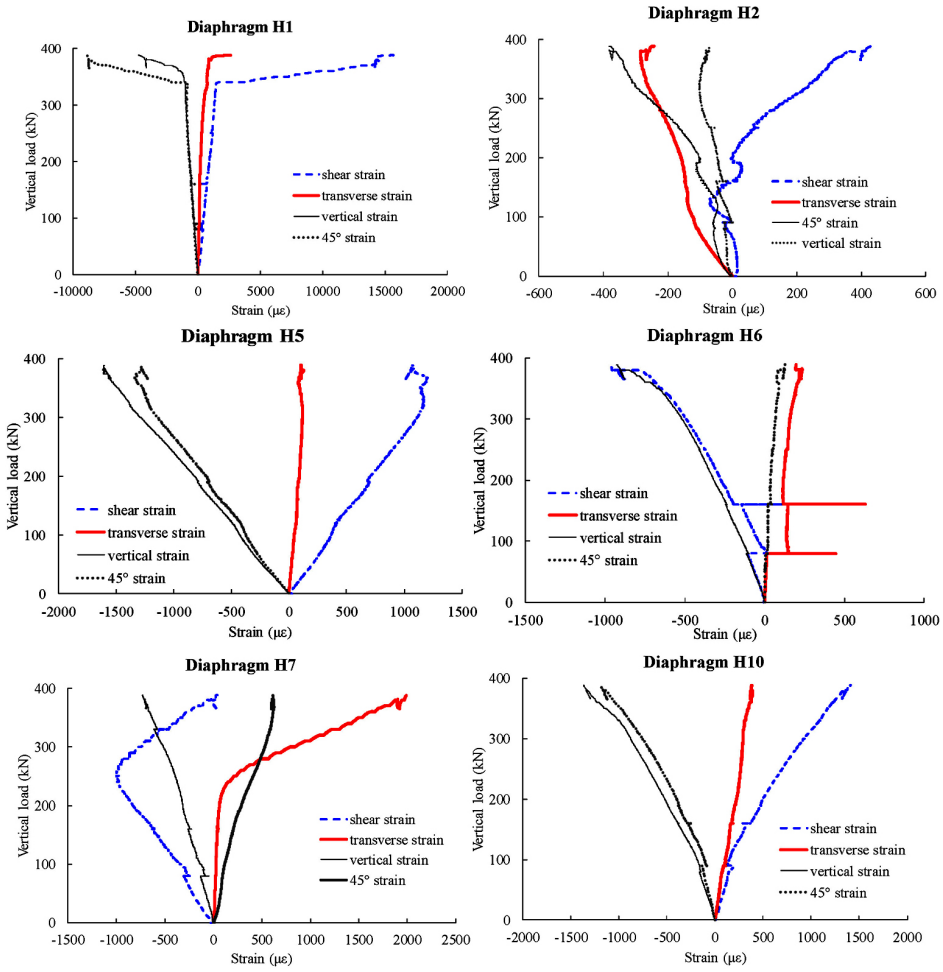

Fig. 11. Load-strain results of transverse diaphragms

Figure 13 gives the load-strain results of top flanges and top connecting plates near bolts. Under the compressive stress, the top flanges of adjacent segments support each other. As shown in the figure, the stress on the outer panel is relatively small, indicating that the bolts were subjected to small shear forces. The strain of the top plate near the bolt hole has not reached the yield strain and is still within the elastic range, indicating that the mother plate at this position were not subjected to large punching shear stress.

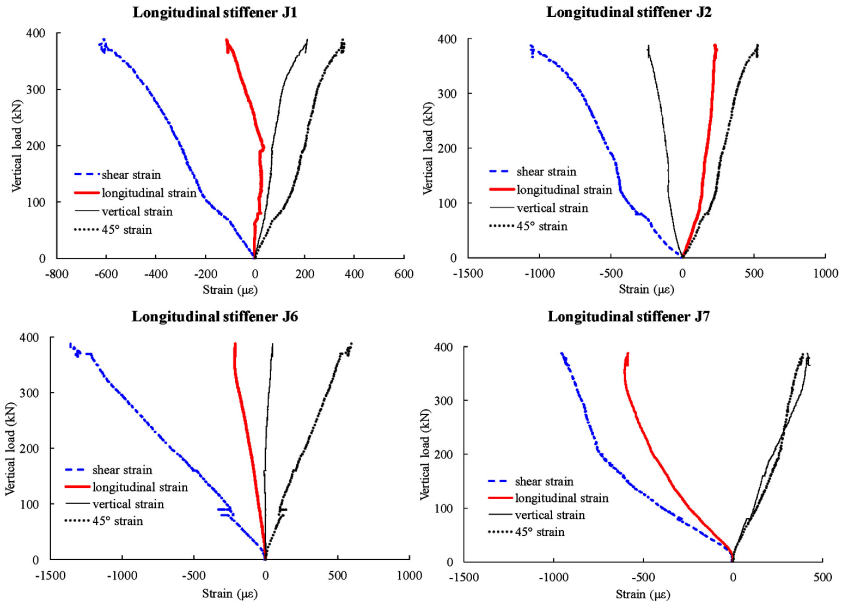

Fig. 12. Load-strain results of longitudinal stiffeners

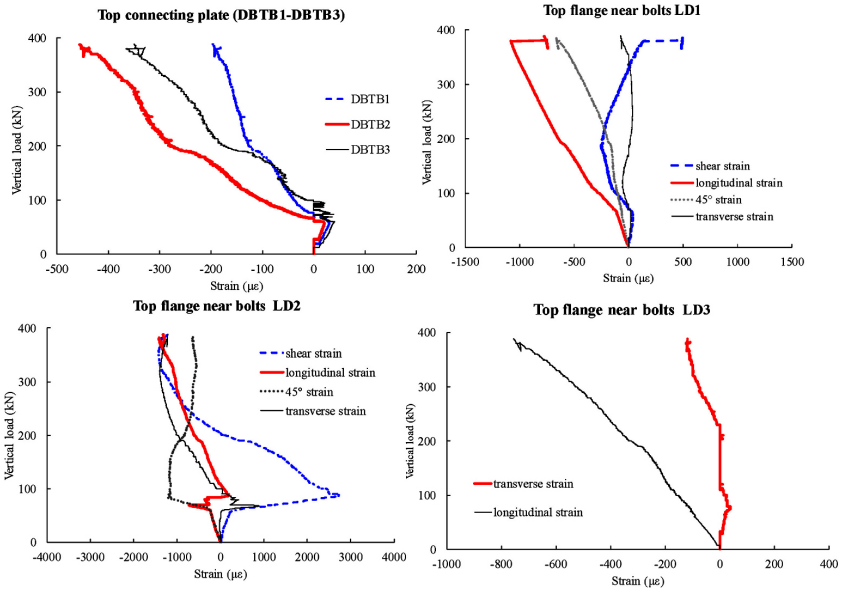

Fig. 13. Load-strain results of top flanges and top connecting plates near bolts (Annotation: 45°strain gage of CD3 is open circuit)

Figure 14 gives Load-strain results of bottom flanges and bottom connecting plates near bolt. As the loading progresses, there is a noticeable gap opening phenomenon from the bottom of the joint surface. As shown in the figure, the bottom connecting plates near bolts near the bolt hole has generated significant plastic strain, and many measuring points have exceeded the strain gauge range (20000 με). The strain on the bottom flanges near the bolt hole is even greater, and a large number of measuring points exceed the range of the strain gauge, even causing the strain gauge to be pulled out and causing the circuit, making it impossible to read strain data normally. The bottom flanges near the bolt hole eventually undergoes serious punching and cutting damage, causing a sharp decrease in the load capacity of the component.

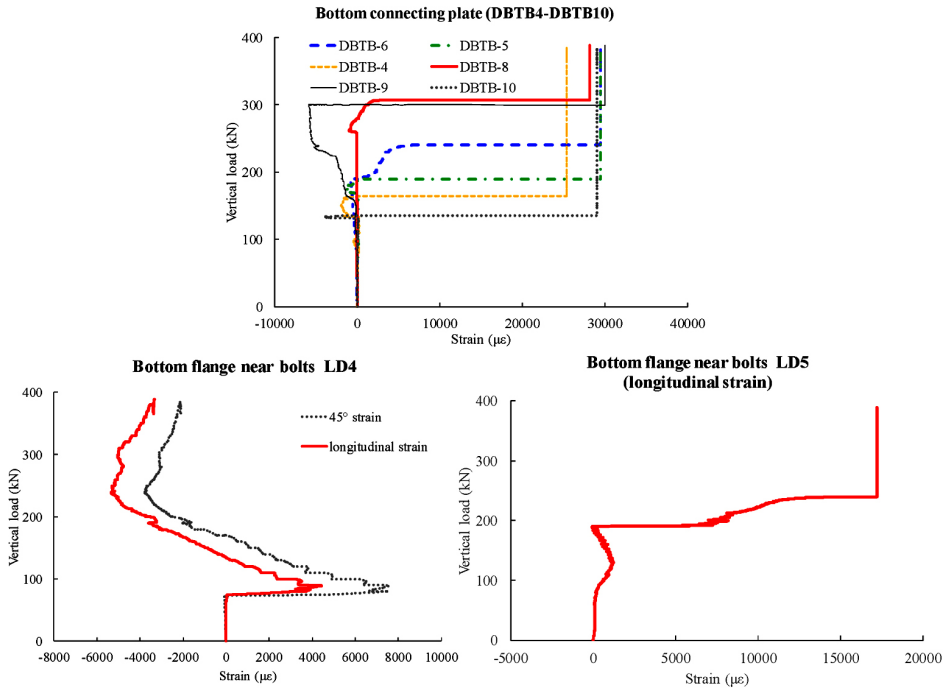

Fig. 14. Load-strain results of bottom flanges and bottom connecting plates near bolts (Annotation: transverse strain gage of LD4 is open circuit)

Figure 15 gives load-strain results of left webs and left connecting plates near bolt. The measurement points TBZC3 and TBZC4 on the left connecting plates near the bolt hole on the lower side of the section show greater strain compared to the TBZC1 and TBZC2 on the upper side, indicating that the bolt shear force is greater in the tensile zone and smaller in the compressive zone. Similarly, the strain of the left webs LCZ1–LCZ3 near the bolt holes on the upper side of the section is relatively small and still in an elastic state, while LCZ5–LCZ6 on the tensile side shows obvious plastic deformation, and some of the mother

plates at these positions have also undergone severe punching deformation and even been pulled apart. As given in Figure 16, the strain distribution and variation patterns of right webs and left connecting plates near bolt are very similar with the those on the left side, and will not be repeated here.

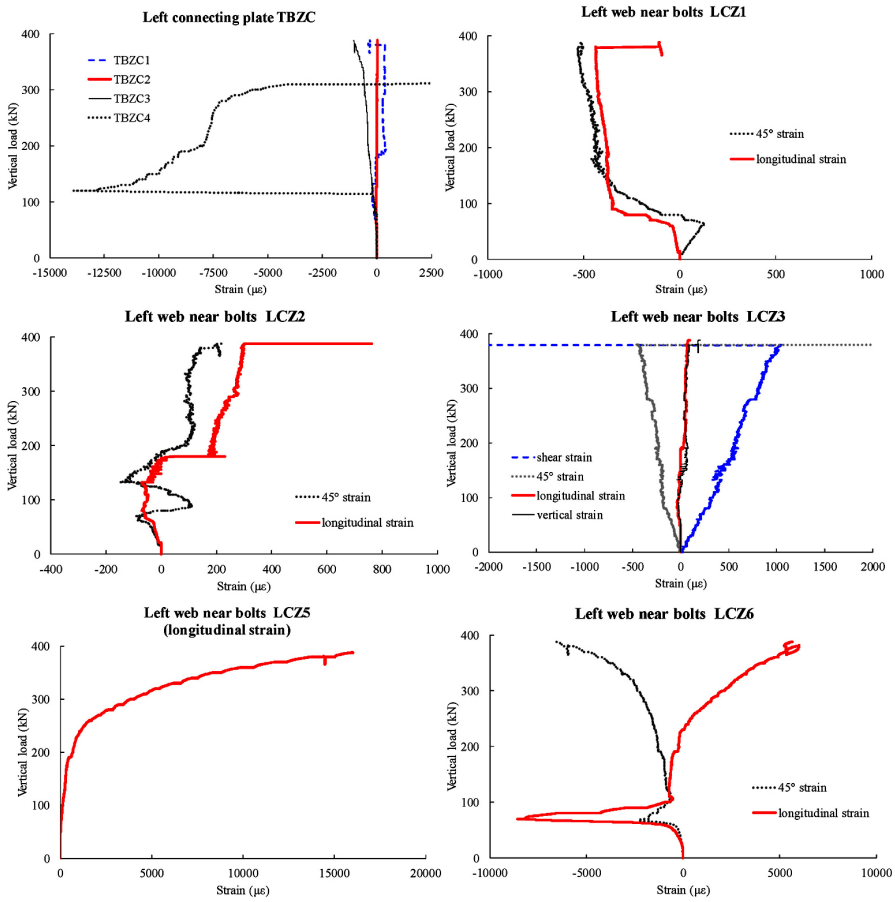

Fig. 15. Load-strain results of left webs and left connecting plates near bolts (Annotation: vertical strain gages of LCZ1, LCZ2, LCZ6 are open circuit)

In summary, the strain results of this experiment truly and completely reflect the actual stress state and variation law of each measuring point. Among them, the strain of measuring points far away from the bolt holes increases linearly with the load, while the strains of measuring points near the bolt holes change irregularly. This is due to manufacturing errors, and each bolt hole is gradually clamped during the loading process. Therefore, the stress near the joint surface continuously redistributes in each bolt hole.

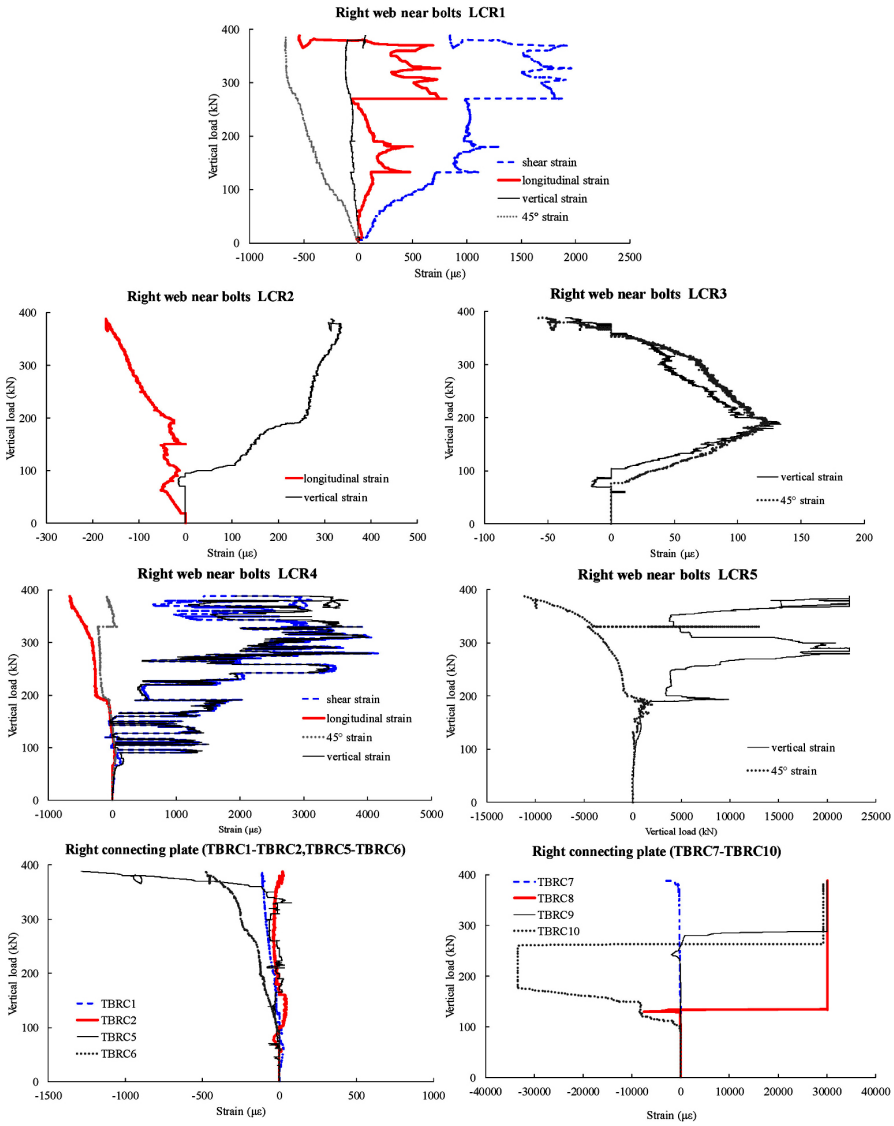

Fig. 16. Load-strain results of right webs and right connecting plates near bolts (Annotation: longitudinal strain gages of LCR3, LCR5, 45°strain gage of LCR2 are open circuit)

3.3. Vertical load-joint gap width results

Because the 1/4 scale member cannot enter the manhole for welding during manufacturing, the construction difficulty is greater than that of the full scale member. Thurs, due to processing errors, the joint gap width has an initial gap width of 2.5 mm in the initial state. During the step-by-step loading process, the gap width of the joint continuously increases.

Since there is obvious asymmetry during the test loading, the joint gap width and deflection of the connection point on the left side are significantly larger. Here, the vertical load-joint gap width curve is given in Figure 17. Throughout the loading process, there is a certain fluctuation in the gap width, but the overall growth shows a linear change. When the load reaches 388kN, the specimen is entirely damaged, and the gap width instantly increases. Finally, the gap width of the joint reaches 3.7 cm.

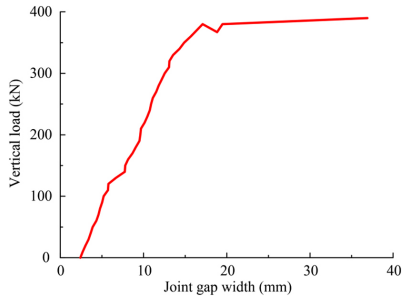

Fig. 17. Vertical load-joint gap width curve

3.4. Damage situation of test components

Figures 18 and 19 respectively give the photos of bolt failure and mother plates damage. The bolt of the right web was sheared and damaged when loaded to 380 kN, indicating that a significant shear stress occurred near the bottom plate on the right side. The failure cross section of bolt is neat, and the right web underwent significant punching deformation. When the test load reached 388 kN, the bottom flanges near the bolt holes were completely cut and damaged, forming the U-shaped failure gap. Below the axis of the left web, significant tensile stress was applied and significant punching deformation occurred, with bolt holes on the left web being damaged by punching.

Fig. 18. Photos of bolt failure

Fig. 19. Photos of mother plates failure

4. Conclusions

This article takes the segmental-assembled steel temporary beam buttress as the research object, designs and processes a 1:4 scaled test specimen. The overall mechanical state and failure mode of test specimen were obtained under vertical force through static test loading. The following conclusions can be drawn:

1. The vertical load-displacement curve of the specimen was obtained through the experiment, and the ultimate bearing capacity and overall stiffness changes of the specimen were obtained. The structure did not experience local buckling or overall instability, and the overall structural performance was strong. The ultimate load-bearing capacity of the scaled test model is 388 kN. The ultimate bearing capacity of the actual full-size temporary beam buttress can be calculated as 16 times of the test result according to the similarity ratio.
2. The joint surface of the test specimen is the weak position. Since the construction difficulty for the 1/4 scale test specimen, the manufacturing errors occurred and the joint surfaces after loading on both sides show obvious asymmetry. The joint surface on the left side has a significant downward deflection and more severe damage.
3. The main failure mode of the test specimen is the punching and shearing failure of the steel plates near the bolt hole caused by the continuous increase in joint gap width. It is indicated that the bending resistance of the joint is relatively low and needs to be properly strengthened during the design process.

In the future, it is urgent to conduct the numerical simulation analysis based on the test results.

Further, the effect of different reinforcement measures, such as increasing the distance from the bolt hole to the edge of the segment, thickening the steel plate at the edge of the segment, and increasing the bolt diameter and grade, needs to be studied in-depth. To ensure the fatigue safety of the steel temporary beam buttress, the fatigue performance under the cyclic load of trains during the service life will be studied.

Acknowledgements

The study described in this paper was supported by the programs of National Natural Science Foundation of China (Grant No. 52308537), Zhejiang Provincial Natural Science Foundation of China (Grant No. LQ24E080023) and China Postdoctoral Science Foundation (Grant No. 2023M730154). The support extended is gratefully acknowledged by the authors.

References

[1] M.F. Báez H., A. Fraile, J. Fernández, and L. Hermanns, "A vibration prediction model for culvert-type railroad underpasses", *Engineering Structures*, vol. 172, pp. 1025–1041, 2018, doi: 10.1016/j.engstruct.2018.06.025.

[2] F.F. Guo, Y.P. Chen, Y.J. Zhang, et al., "Safety assessment of the construction of double track tunnels undernear existing railway tunnels", *Archives of Civil Engineering,* vol. 70, no. 1, pp. 375–387, 2024, doi: 10.24425/ace.2024.148917.

[3] TB 10002-2017 Code for Design on Railway Bridge and Culvert. Beijing, China Railway Publishing House, 2017 (in Chinese).

[4] TB 10092-2017 Code for Design of Concrete Structures of Railway Bridge and Culvert. Beijing, China Railway Publishing House, 2017 (in Chinese).

[5] China Railway Corporation, "Railway Technical Management Regulations". Beijing, China Railway Publishing House, 2014 (in Chinese).

[6] T.Q. Wu, "Study on key points of design and construction of temporary beam buttress", *Vualure Engineering*, vol. 42, no. 14, pp. 88–90, 2023, doi: 10.3969/j.issn.1006-4311.2023.14.027 (in Chinese).

[7] Z.F. Sun, "Design and research of large span steel box portal pier for high speed railway", *Journal of Railway Engineering Society*, vol. 36, no. 4, pp. 43–47, 2019, doi: 10.3969/j.issn.1006-2106.2019.04.009 (in Chinese).

[8] R. Tao and X.H. Chen, "Design and research on steel portal pier of railway bridge", *Railway Standard Design*, vol. 64, no. S1, pp. 163–167, 2020, doi: 10.13238/j.issn.1004-2954.202008180007 (in Chinese).

[9] C.C Chou and Y.C. Chen, "Cyclic tests of post-tensioned precast CFT segmental bridge columns with unbonded strands", *Earthquake Engineering and Structural Dynamics*, vol. 35, no. 2, pp. 159–175, 2006, doi: 10.1002/eqe.512.

[10] K.D. Zhang, J.F. Jia, Y.L. Bai, et al., "Design and seismic performance of precast segmental bridge columns repaired with UHPC jacket after earthquake-induced damage", *Engineering Structures*, vol. 291, art. no. 116442, 2023, doi: 10.1016/j.engstruct.2023.116442.

[11] J.F. Jia, B. Wei, Y.L. Bai, S.W. Wu, et al., "Seismic performance of precast segmental bridge columns reinforced with both stainless-steel bars and GFRP bars", *Journal of Bridge Engineering*, vol. 27, no. 1, 2022, doi: 10.1061/(ASCE)BE.1943-5592.0001810.

[12] J.W. Fan, L. Yang, Y.Q. Wang, et al., "Research on axial loading behaviour of deconstructable bolt spliced square steel tubular columns", *Journal of Building Structures*, vol. 43, no. 10, pp. 307–319, 2022, doi: 10.14006/j.jzjgxb.2021.0194 (in Chinese).

[13] TB 10091-2017 Code for Design on Steel Structure of Railway Bridge. Beijing, China Railway Publishing House, 2017 (in Chinese).

[14] T. Wang, X. Xie, C. Shen, and Z. Tang, "Effect of hysteretic models on elasto-plastic seismic performance evaluation of a steel arch bridge", *Earthquake Structures*, vol. 10, no. 5, pp. 1089–1109, 2016, doi: 10.12989/eas.2016.10.5.1089.

[15] H.Q. Zhuge and X. Xie, "Hysteresis model for fiber elements in effective damaged zone of square-section steel piers considering local instability effect of steel plates", *Journal of Structural Engineering*, vol. 146, no. 8, 2020, doi: 10.1061/(ASCE)ST.1943-541X.0002698.

Received: 2024-04-27, Revised: 2024-06-27